

A search for starlight reflected from HD 75289 b

Christopher Leigh¹, Andrew Collier Cameron¹, Stephane Udry², Jean-François Donati³, Keith Horne¹, David James⁴ and Alan Penny⁵

¹ University of St Andrews, St Andrews, Fife, KY16 9SS, U.K

² Observatoire de Genève, 51 ch. des Maillettes, 1290 Sauverny, Switzerland

³ Laboratoire d'Astrophysique Observatoire Midi-Pyrénées, 14 avenue Edouard Belin, F-31400 Toulouse, France

⁴ Observatoire de Grenoble, F-38041 Grenoble, Cedex 9, France

⁵ Rutherford Appleton Laboratory, Chilton, Didcot, Oxon, OX11 0QX, U.K

29 October 2018

ABSTRACT

We have used a doppler tomographic analysis to conduct a deep search for the starlight reflected from the planetary companion to HD 75289. In 4 nights on VLT2/UVES in January 2003, we obtained 684 high resolution échelle spectra with a total integration time of 26 hours. We establish an upper limit on the planet's geometric albedo $p < 0.12$ (to the 99.9% significance level) at the most probable orbital inclination $i \simeq 60^\circ$, assuming a grey albedo, a Venus-like phase function and a planetary radius $R_p = 1.6R_{Jup}$. We are able to rule out some combinations of the predicted planetary radius and atmospheric albedo models with high, reflective cloud decks.

Key Words: Planets: extra-solar - Planets: atmosphere - Stars: HD 75289

1 INTRODUCTION

The existence of a close planetary companion to the G0V star HD75289 was first reported by Udry et al. (2000). In common with 19 of the 117 extrasolar planets known, HD75289b is found to orbit within 0.1 AU of its parent star. Confirmation of the gas-giant nature of the close-orbiting exoplanet, HD209458b (Charbonneau et al. 2000; Henry et al. 2000), suggests that similar objects may reflect enough starlight to allow a direct planetary detection. Spectral models of these ‘‘Pegasi planets’’ (Barman et al. 2002; Sudarsky, Burrows & Hubeny 2003) show that scattered starlight dominates over thermal emission at optical wavelengths. Sudarsky, Burrows & Hubeny (2003) suggest the high effective temperature and relatively low surface gravity of HD75289b may favour the formation of relatively bright, high-altitude silicate cloud decks, which act to scatter starlight back into space before being absorbed by alkali metals in the deeper atmosphere.

Here we report the results of observations, conducted over 4 nights in January 2003 on VLT2/UVES échelle spectrograph, aimed at detecting the starlight reflected from HD75289b. In Section 2 we summarise the basic physics which underpins our analysis, whilst sections 3 and 4 review the acquisition, reduction and processing of the raw échelle spectra, using techniques described more comprehensively in Collier Cameron et al. (2002) and Leigh et al. (2003). Finally, in section 5 we use our results to place upper limits on the grey geometric albedo of the planet.

2 SYSTEM PARAMETERS

HD75289 (HIP43177) is a G0 main sequence star with parameters listed in Table 1. High-precision radial-velocity (RV) measurements obtained between Nov 1998 and Oct 1999 (Udry et al. 2000) were used to identify a planetary companion HD75289b, whose properties (as determined directly from RV studies or inferred using the estimated stellar parameters) are also summarised in Table 1. Since the planet publication (Udry et al. 2000), the orbital solution has been updated with new Coralie RV measurements using a weighted cross-correlation scheme (Pepe et al. 2002) with an appropriate template.

As the planet orbits its host star, some of the starlight incident upon its surface is reflected towards us, producing a potentially detectable signature within the observed spectra of the star. This signature takes the form of faint copies of the stellar absorption lines, Doppler shifted due to the planet's orbital motion and greatly reduced in intensity due to the small fraction of starlight the planet intercepts and reflects back into space.

With our knowledge of the stellar mass and the planet's orbital period we can estimate the orbital velocity of the planet V_p (see Collier Cameron et al. 2002). The apparent RV amplitude K_p of the reflected light is given by

$$K_p = V_p \sin i = 147 \sin i \text{ km s}^{-1}, \quad (1)$$

where the orbital inclination i is, according to the usual convention, the angle between the orbital angular momentum vector and our line of sight.

Star :	
Spectral Type	G0V ¹
m_v	6.35 (0.013) ^{2,3}
Distance (pc)	28.9 (0.46) ²
T_{Eff} (K)	6135 (40) ⁴
M_* (M_\odot)	1.22 (0.05) ^{5,6,7}
R_* (R_\odot)	1.25 (0.05) ^{5,6,7}
[Fe/H]	0.27 (0.06) ⁴
P_{rot} (d)	16.0 (3.0) ^{8,9}
$v \sin i$ (km s^{-1})	3.8 (0.6) ¹⁰
Age (Gyr)	5.6(1.0) ^{8,11}
Planet :	
Orbital Period P_{orb} (d)	3.5091 (0.0001) ¹⁰
Transit Epoch T_0 (JD)	52651.1566 (0.1251) ¹⁰
K_* (m s^{-1})	53.4 (0.6) ¹⁰
a (AU)	0.0483 (0.0020) ¹⁰
$M_p \sin i$ (M_{Jup})	0.455 (0.028) ¹⁰

Table 1. System parameters (and uncertainties) for HD75289 and its planetary companion. ¹ Gratton, Focardi & Bandiera (1989), ² ESA. (1997), ³ Gray, Napier & Winkler (2001), ⁴ Santos, Israelian & Mayor (2001), ⁵ Fuhrmann, Pfeiffer & Bernkopf (1998), ⁶ Gonzalez & Laws (2000), ⁷ Gonzalez et al. (2001), ⁸ Udry et al. (2000), ⁹ Noyes et al. (1984), ¹⁰ Udry et al. (2000) revised for this paper, ¹¹ Donahue (1993).

For all but the lowest inclinations, the orbital velocity amplitude of the planet is much greater than the broadened widths of the stellar absorption lines. Hence, lines in the reflected-light spectrum of the planet should be Doppler shifted well clear of their stellar counterparts, allowing a clean spectral separation for most of the orbit.

By isolating the reflected planetary signature, we are in effect observing the planet-star flux ratio (ϵ) as a function of orbital phase (ϕ) and wavelength (λ), where

$$\epsilon(\alpha, \lambda) \equiv \frac{f_p(\alpha, \lambda)}{f_*(\lambda)} = p(\lambda)g(\alpha, \lambda)\frac{R_p^2}{a^2}. \quad (2)$$

The phase function $g(\alpha, \lambda)$ describes the variation in the planet-star flux ratio with the phase angle α , here α is the angle subtended at the planet by the star and the observer, and varies as $\cos \alpha = -\sin i \cos \phi$. As the shape of $g(\alpha, \lambda)$ is unknown, current practice is to adopt a specific phase function in order to express the results in terms of the planet-star flux ratio that would be seen at phase angle zero

$$\epsilon_0(\lambda) = p(\lambda)\frac{R_p^2}{a^2}, \quad (3)$$

where $p(\lambda)$ is the wavelength-dependent geometric albedo and the orbital distance a is constrained by Kepler's third law. For reasons described in Collier Cameron et al. (2002) and Leigh et al. (2003), the $g(\alpha, \lambda)$ we adopt is a polynomial approximation to the empirically determined phase function for Venus (Hilton 1992).

In the event of a planet detection, analysis of the data should allow us to determine two fundamental properties:

- (i) K_p , the planet's projected orbital velocity, from which we obtain the system inclination and planet mass, since $M_p \sin i$ is known from the star's Doppler wobble,
- (ii) ϵ_0 , the maximum flux ratio observed where, by making theoretical assumptions about the nature of the planet, we can invoke equation (3) to constrain R_p or p .

UTC start	Phase	UTC End	Phase	N_{exp}
Jan 14 01:00:04	0.396	Jan 14 09:29:44	0.497	188
Jan 15 00:56:42	0.680	Jan 15 09:21:32	0.780	173
Jan 21 02:40:18	0.410	Jan 21 09:34:54	0.492	183
Jan 22 03:35:30	0.706	Jan 22 09:41:01	0.778	140

Table 2. Journal of observations. The UTC mid-times and orbital phases are shown for the first and last spectral exposures secured on each night of observation in January 2003. The number of exposures is given in the final column.

3 OBSERVATIONS

We observed HD75289 during Jan 2003 using the blue arm of the UV-Visual Échelle Spectrograph (UVES), mounted on the 8.2-m VLT/UT2 (Kueyen) telescope at the Paranal Observatory in Chile. The detector was a single EEV CCD-44 array windowed to an image format of 2048×3000 $15.0 \mu\text{m}$ pixels, and centred at 475.8 nm in order 102 of the 41.6 g mm^{-1} échelle grating, giving good wavelength coverage from 406.5 nm to 522.0 nm. For reasons described in greater detail in Collier Cameron et al. (2002), we believe the prominence of Rayleigh scattering, combined with the high density of absorption lines within this spectral range, offer the best chance of detection. With an average pixel spacing close to 1.5 km s^{-1} , the FWHM intensity in the central orders of the thorium-argon calibration spectra was found to be 4.5 pixels, suggesting an effective resolving power $R = 43000$.

Table 2 details the 4 nights of observations that contribute to this analysis. Each of the stellar spectra were exposed between 100s and 300s, depending upon the seeing, in order to expose the CCD to $\sim 40000 \text{ ADU pix}^{-1}$ in the brightest parts of the image. A typical exposure in average seeing (0.8 arcsec) yielded $\sim 4 \times 10^5$ electrons per pixel step in wavelength in the brightest orders after extraction. The CCD's 7s fast-readout time allowed an observing efficiency $> 90\%$, and saw a gain of 2.4 and readout noise of $\sim 6 e^-$.

4 DATA PROCESSING

One-dimensional spectra were extracted from the raw images using an automated pipeline reduction system built around the Starlink ECHOMOP and FIGARO packages.

After initial tracing of the échelle orders, an extraction process subtracted the bias from each frame, cropped it, determined the form and location of the stellar profile on each image, subtracted a linear fit to the scattered-light + sky background across the spatial profile, and performed an optimal (profile and inverse variance-weighted) extraction of orders across the full spatial extent of the object+sky region. In all, 25 orders (Nos 90-114) were extracted from each image, giving good spectral coverage from 406.5 to 522.0 nm. Following extraction, the S:N in the continuum of the brightest orders was typically 650 per pixel step.

Flat-field balance factors were applied prior to extraction by summing the 50-100 flat-fields taken at the start and end of each night. Although the UVES instrument was very stable between observations, we found that the noise was slightly reduced ($\sim 2\%$) by the use of nightly flat-fields rather than master flat-fields combining all 4 nights' data.

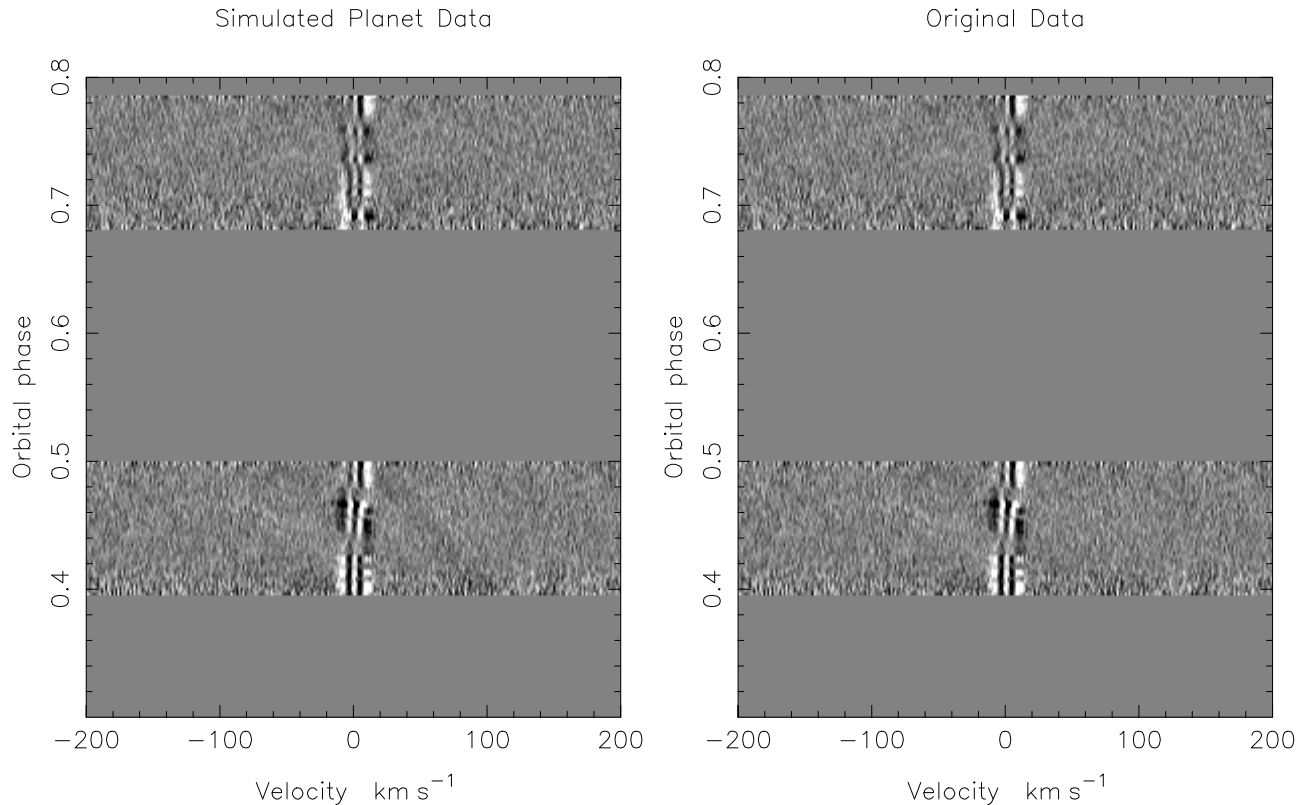


Figure 1. Time series of deconvolved profiles derived from the VLT/UVES spectra, secured over 4 nights in Jan 2003. The left plot (a) demonstrates the result of adding a simulated planet signal at an inclination of 80° , assuming grey geometric albedo $p = 0.4$ and a radius, $1.6 R_{Jup}$. The planetary signature appears as a dark sinusoidal feature crossing from right to left as phase increases and centred on the superior conjunction at phase 0.5. The right plot (b) shows the original data, where no such trail is evident. The greyscale runs from black at -10^{-4} times the mean stellar continuum level, to white at $+10^{-4}$. The velocity scale is in the reference frame of the star.

4.1 Extracting the planet signal

The first step in extracting the reflected component is to subtract the direct stellar component from the observed spectrum. The planet signal should then consist of faint Doppler-shifted copies of each of the stellar absorption lines, at this stage buried deeply in the noise. A detailed description of this procedure is given in Collier Cameron et al. (2002) Appendix A. After cleaning any correlated fixed-pattern noise remaining in the difference spectra (see Collier Cameron et al. (2002) Appendix B), we create a composite residual line profile by deconvolving each residual spectra with a list of stellar absorption line strengths (Collier Cameron et al. (2002) Appendix C). The deconvolution results in a 32-fold improvement in the S:N, by combining the properties of 2360 images of 1744 absorption lines listed within the observed wavelength range. The composite line profiles are then stacked by phase to display temporal variations in brightness and RV, as at Fig. 1. Any planet signal present appears as a dark sinusoidal feature in velocity space centred on the superior conjunction at phase 0.5.

The central pattern of distortions in Fig. 1 is consistent with sub-pixel shifts in the position of the stellar spectra with respect to the detector over the course of the night. Fortunately they only affect a range of velocities at which the planet signature would in any case be indistinguishable from that of the star.

4.2 Simulated planet signatures

We verified that a planetary signal is preserved through the above sequence of operations, in the presence of realistic noise levels, by adding a simulated planetary signal to the observed spectra (Fig. 1a). The fake signal also acts to calibrate the strength of any genuine observations and the associated confidence contours. Detailed explanations of the simulated planet calibration can be found in Collier Cameron et al. (2002) and Leigh et al. (2003). To ensure a strong signal we used a simulated planet of radius $1.6 R_{Jup}$ and wavelength-independent geometric albedo $p = 0.4$, which when viewed at zero phase angle should give a planet-star flux ratio $\epsilon_0 = f_p/f_* = 9.71 \times 10^{-5}$.

Except for the case of a tidally locked system, any relative motion between the surface of the planet and the surface of the star will result in a difference between the line widths of the incident and reflected spectra. From the known stellar parameters (Table 1), we have conducted Monte Carlo trials to estimate that the reflected component within the HD75289 spectra will exhibit typical line widths close to 13 km s^{-1} . In order to correctly mimic the reflected starlight we have selected the faster rotating G0V star HD1461 as our planetary template. A star which is of very similar temperature and elemental abundance to HD75289.

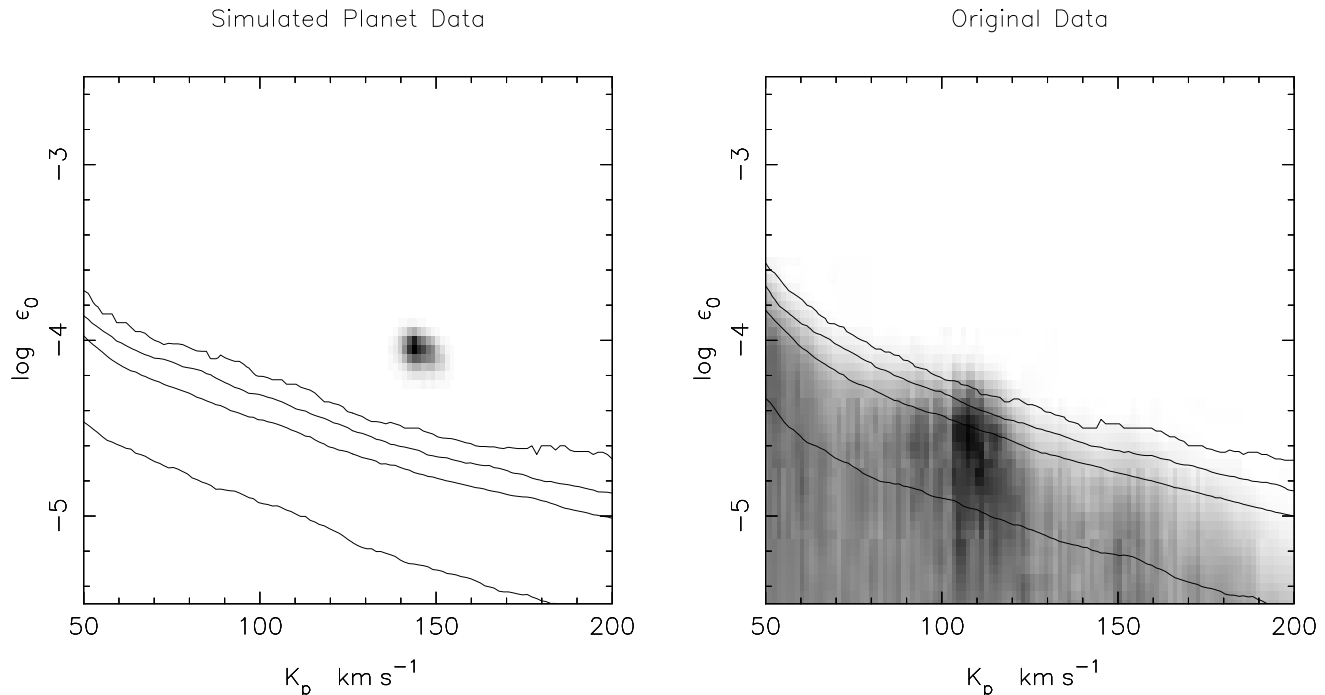


Figure 2. Relative probability map of model parameters K_p and $\log \epsilon_0 = \log p(R_p/a)^2$, derived from the VLT/UVES observations of HD75289. The greyscale denotes the probability relative to the best-fit model, increasing from 0 for white to 1 for black. The contours show the confidence levels at which spurious detections due to non-Gaussian noise can be ruled out. From top to bottom, they show the 99.9%, 99.0%, 95.4% and 68.3% confidence limits on ϵ_0 for fixed K_p . The left plot (a) demonstrates how the simulated planet signal is recovered through the analysis with ease, and is detected well above the 99.9% confidence limit. The right plot (b) containing the original data, however, demonstrates little evidence for a planetary detection. It is important to note that the contours only give the probability of a false detection if the value of K_p is known in advance, which is not the case here. The slightly increased probability density seen close to $K_p = 110 \text{ km s}^{-1}$ (within the K_p distribution predicted by Leigh, Collier Cameron & Guillot 2003) returns a large false-alarm probability of 32% when considering all plausible values $35 < K_p < 147 \text{ km s}^{-1}$, which is far too uncertain to claim as genuine.

4.3 Matched Filter Analysis

The next step involved a matched-filter analysis, described by Collier Cameron et al. (2002) Appendix D, to search for features in the time-series of composite residual profiles whose temporal variations in brightness and RV resemble those of the expected reflected-light signature.

The relative probabilities of the χ^2 fits to the data for different values of the free parameters R_p/a and K_p are conveniently displayed in greyscale form as a function of K_p and $\log \epsilon_0 = \log p(R_p/a)^2$. Fig. 2 details the probability map for the simulated (a) and original (b) observations, normalised to the $\Delta\chi^2$ of the best-fit model.

To set an upper limit on the strength of any planet signal, or to assess the likelihood that any signal detection is spurious, we need to compute the probability of obtaining similar improvements in χ^2 by chance alone. We achieve this using a “bootstrap” procedure to construct empirical distributions for confidence testing, using the data themselves. In 3000 trials, we randomized the order in which the 684 observations were secured, but associated them with the original sequence of dates and times. Genuine signals are scrambled in phase, but re-ordered data are as capable as the original data of producing spurious detections through chance alignments of systematic errors along a sinusoidal path through the data. We record the least-squares estimates of $\log \epsilon_0$ and the associated χ^2 as functions of K_p in each trial.

The percentage points of the resulting bootstrap distribution are shown as contours in Fig. 2. From bottom to top, the contours represent the 68.4%, 95.4%, 99.0% and 99.9% bootstrap upper limits on the strength of the planet signal. Thus the 99.9% contour represents the value of $\log \epsilon_0$ that was only exceeded in 3 of the 3000 trials at each K_p .

5 RESULTS

The results of this analysis appear in the form of a relative probability map of model parameters K_p and $\log \epsilon_0 = \log p(R_p/a)^2$, shown at Fig. 2. The calibrated confidence contours allow us to apply constraints to the geometric albedo of the planet, given certain theoretical assumptions about the system.

5.1 Upper Limits on Grey Albedo

The grey albedo model makes the unlikely assumption that the planet-star flux ratio remains independent of wavelength. By adopting a theoretical radius for the planet we can use equation (3) to constrain its geometric albedo. Fig. 3 details the upper limits on the albedo at the 99.9% level of significance, for a range of possible inclinations and radii.

We find that the albedo limits are less strongly constrained with low inclination systems. This is a natural con-

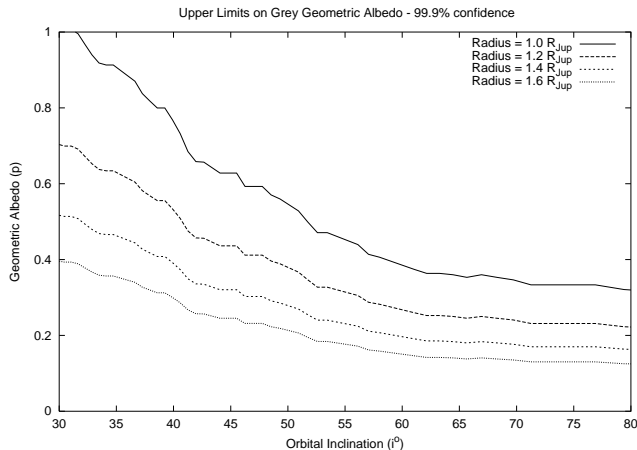


Figure 3. Upper limits (99.9% confidence) on the geometric albedo p as a function of inclination and radius, assuming the atmosphere of the planet imposes no wavelength dependence on reflected light, i.e. a grey albedo model. The contours, from top to bottom, represent upper limits assuming theoretical radii for the orbiting planet of 1.0, 1.2, 1.4 and 1.6 R_{Jup} , covering orbital inclinations $30^\circ < i < 80^\circ$. If the planet exhibits the radius, 1.6 R_{Jup} , and inclination, $i = 75^\circ$, predicted by Leigh, Collier Cameron & Guillot (2003), then our observations suggest we can be 99.9% confident of a grey geometric albedo $p < 0.12$.

sequence of the matched-filter analysis, where fitting such models incorporate more pixels close to the noisier ripples in the central stellar region of the deconvolved profile.

If we adopt the Leigh, Collier Cameron & Guillot (2003) theoretical radius for HD75289b of $R_p = 1.6 R_{Jup}$, we find the planet-star flux ratio, at the most probable $K_p \simeq 127 \text{ km s}^{-1}$, is constrained to $f_p/f_* < 4.18 \times 10^{-5}$ at the 99.9% level, i.e. a geometric albedo less than 0.12. This would strongly rule out atmospheric models which incorporate high-altitude, reflective cloud decks such as the Class V model of Sudarsky, Burrows & Pinto (2000).

6 CONCLUSION

We have observed HD75289 over 4 nights in Jan 2003, using the VLT2/UVES instrument, in an attempt to detect starlight reflected by the known close-orbiting planetary companion. The excellent stability of the spectrograph, combined with the reasonable observing conditions, have enabled us to produce deep upper limits on the geometric albedo of the planet. In truth, with our knowledge of the system and current theoretical predictions, we would have expected a reasonably unambiguous detection of the planet. However, we find very little evidence to suggest its presence. Possible reasons for the discrepancy are,

(i) The inclination of the system is such that the spectral features of the planet do not cleanly separate from the stellar features. i.e. maximum Doppler shift is not sufficient to disentangle the planets signal. However, evidence generated (Leigh, Collier Cameron & Guillot 2003) using the known system parameters, suggests an inclination $i \gg 20^\circ$.

(ii) Our choice of phase function $g(\alpha, \lambda)$ is wrong. It may be that close-orbiting Pegasi planets are less prone to back-scatter incoming starlight than we see with Jupiter or Venus (Hovenier 1989; Seager, Whitney & Sasselov 2000).

(iii) Although the transiting planet HD209458 has indicated the presence of a gas giant, it may be that HD75289b is a more compact terrestrial planet reflecting substantially less starlight (see Guillot et al. 1996).

(iv) It could be that the geometric albedo is inherently low (cf. Class IV CEGP of Sudarsky, Burrows & Pinto 2000), with starlight absorbed deep in the atmosphere of a planet where no high-level clouds are present to reflect the incident light. However, at the wavelengths observed, we do expect a more significant contribution from Rayleigh scattering.

Whatever the cause, these observations provide a strong test for developing theoretical models which aim to predict the atmospheric nature of these objects. This is a field in desperate need of continued observations on the brightest of these Pegasi planets, as are detailed in the work of Leigh, Collier Cameron & Guillot (2003).

REFERENCES

- Barman T., Hauschildt P., Schweitzer A., Stancil P., Baron E., Allard F., 2002, *ApJ*, 569, 51
- Charbonneau D., Brown T., Latham D., Mayor M., 2000, *ApJ*, 529, 45
- Collier Cameron A., Horne K., Penny A., Leigh C., 2002, *MNRAS*, 330, 187
- Donahue R., 1993, PhD thesis, New Mexico State Univ.
- ESA., 1997, The Hipparcos catalogue. ESA SP-1200
- Fuhrmann K., Pfeiffer J., Bernkopf J., 1998, *Astronomy and Astrophysics*, 336, 942
- Gonzalez G., Laws C., 2000, *AJ*, 119, 390
- Gonzalez G., Laws C., Tyagi S., Reddy B., 2001, *AJ*, 121, 432
- Gratton R., Focardi P., Bandiera R., 1989, *MNRAS*, 237, 1085
- Gray R., Napier M., Winkler L., 2001, *AJ*, 121, 2148
- Guillot T., Burrows A., Hubbard W., Lunine J., Saumon D., 1996, *ApJ*, 459, 35
- Henry G., Marcy G., Butler P., Vogt S., 2000, *ApJ*, 529, 41
- Hilton J., 1992, Explanatory supplement to *Astronomical Almanac*. University Science Books, Mill Valley, CA
- Hovenier J., 1989, *Astronomy and Astrophysics*, 214, 391
- Leigh C., Collier Cameron A., Guillot T., 2003, *MNRAS*, *MNRAS accepted*, astro-ph/0308414
- Leigh C., Collier Cameron A., Horne K., Penny A., James D., 2003, *MNRAS*, 344, 1271
- Noyes R., Hartmann L., Baliunas S., Duncan D., Vaughan A., 1984, *ApJ*, 279, 763
- Pepe F., Mayor M., Galland F., Naef D., Queloz D., Santos N., Udry S., 2002, *Astronomy and Astrophysics*, 388, 632
- Santos N., Israelian G., Mayor M., 2001, *Astronomy and Astrophysics*, 373, 1019
- Seager S., Whitney A., Sasselov D., 2000, *ApJ*, 540, 504
- Sudarsky D., Burrows A., Hubeny I., 2003, *ApJ*, 588, 1121
- Sudarsky D., Burrows A., Pinto P., 2000, *ApJ*, 538, 885
- Udry S., Mayor M., Naef D., Pepe F., Queloz D., Santos N., 2000, *Astronomy and Astrophysics*, 356, 590

ACKNOWLEDGEMENTS

This work is based on observations with the VLT/UT2 (Kueyen) telescope, operated by the European South Observatory at the Paranal Observatory on Cerro Paranal in the Atacama Desert, Chile. All data processing was conducted using Starlink Project supported hardware and software.

ACC and KDH were supported by PPARC Senior Fellowships and CJL by a PPARC Postgraduate Studentship during the course of this work.